



**HAL**  
open science

# 3D RuO<sub>2</sub> Microsupercapacitors with Remarkable Areal Energy

Anaïs Ferris, Sébastien Garbarino, Daniel Guay, David Pech

► **To cite this version:**

Anaïs Ferris, Sébastien Garbarino, Daniel Guay, David Pech. 3D RuO<sub>2</sub> Microsupercapacitors with Remarkable Areal Energy. *Advanced Materials*, 2015, 27 (42), pp.6625 - 6629. 10.1002/adma.201503054 . hal-01872878

**HAL Id: hal-01872878**

**<https://laas.hal.science/hal-01872878>**

Submitted on 12 Sep 2018

**HAL** is a multi-disciplinary open access archive for the deposit and dissemination of scientific research documents, whether they are published or not. The documents may come from teaching and research institutions in France or abroad, or from public or private research centers.

L'archive ouverte pluridisciplinaire **HAL**, est destinée au dépôt et à la diffusion de documents scientifiques de niveau recherche, publiés ou non, émanant des établissements d'enseignement et de recherche français ou étrangers, des laboratoires publics ou privés.

### 3D RuO<sub>2</sub> Micro-Supercapacitors with Remarkable Areal Energy

Anaïs Ferris, Sébastien Garbarino, Daniel Guay,\* and David Pech\*

A. Ferris, Dr. S. Garbarino, Prof. D. Guay  
INRS-Energie, Matériaux, Télécommunications  
1650 boulevard Lionel Boulet, Varennes, QC, J3X 1S2, Canada  
E-mail: guay@emt.inrs.ca

A. Ferris, Dr. D. Pech  
CNRS, LAAS, 7 avenue du colonel Roche, F-31400 Toulouse, France  
Univ de Toulouse, LAAS, F-31400 Toulouse, France  
E-mail: dpech@laas.fr

Keywords: micro-supercapacitor, ruthenium oxide, porous gold, dynamic template

In the last decade, extensive efforts have been devoted to integrated micrometre-sized supercapacitors because of the increasing need for on-board energy supply/storage in wearable micro-electronic devices and embedding wireless sensors networks in our everyday environment.<sup>[1-3]</sup> Compared to micro-batteries, micro-supercapacitors can provide high power delivery and, more importantly, have a much longer operating life time.<sup>[4]</sup> This comes at the expense of a much lower energy density: until now, micro-supercapacitors have fallen far short of powering a wireless sensor node or any micro-electronic device. Moreover, for on-chip applications, areal density is more important than volumetric density due to the limited area available for integrating components into a system. It is therefore crucial to consider the capacitance and the energy of micro-supercapacitors normalized to their footprint areas. To date, despite their excellent power performances, the reported areal capacitance (*i.e.* normalized to the surface area) of micrometre-sized electrical double-layer capacitors typically ranges from 0.4 to 16.5 mF cm<sup>-2</sup>.<sup>[5-12]</sup>

This capacitance could be increased through the utilization of pseudo-capacitive materials, mainly transition metal oxides. These materials' charge storage mechanism relies on rapid and reversible faradaic surface reactions<sup>[13]</sup> and offers a means of achieving high energy density at high charge-discharge rate. The most promising pseudo-capacitor material is hydrous ruthenium dioxide (RuO<sub>2</sub>.xH<sub>2</sub>O) which exhibits high specific capacitance, high

electronic conductivity and long cycle life.<sup>[14]</sup> While its high cost has limited its development for large supercapacitors, the use of this material becomes relevant and promising for micro-supercapacitors.<sup>[15]</sup> Considering the size of the device, the amount of active material involved is limited and cost is mainly determined by the fabrication processes and the assembly of the device. Recently, we reported a specific capacitance of 12.8 mF cm<sup>-2</sup> for a RuO<sub>2</sub>-based micro-supercapacitor.<sup>[16]</sup> Although this capacitance is higher than that obtained with carbonaceous materials, the corresponding areal energy density (0.4 μWh cm<sup>-2</sup>) is still far from that of Li-ion micro-batteries (in the range of mWh cm<sup>-2</sup>). As pseudo-capacitors store their charge in the initial few nanometers from the surface, the performance of micro-supercapacitors is limited by the very thin active layer of electrodes. A three-dimensional array of electrode, with high-aspect-ratio, is therefore necessary to allow more active materials to be loaded per unit area.<sup>[17]</sup> An attractive approach to increasing the capacitance is to deposit the pseudo-capacitive material onto a high surface area structured support.<sup>[18-20]</sup> Capacitances per surface area, exceeding 100 mF cm<sup>-2</sup>, were reported for micro-supercapacitors using such three-dimensional structures.<sup>[21-24]</sup>

In this study, we have fabricated a porous gold/RuO<sub>2</sub> electrode through a two-step procedure, in which the gold current collectors are sculptured using the hydrogen bubble dynamic template synthesis,<sup>[25-27]</sup> followed by the electrodeposition of the hydrous ruthenium oxide. The resulting electrode exhibits unprecedented high capacitance per surface area, in excess of 3 F cm<sup>-2</sup>, and – for the first time – an all-solid-state supercapacitor with a specific energy per surface area comparable to that of lithium-ion micro-batteries has been achieved, but with superior power and cycling stability. Such porous gold/ruthenium oxide hybrid structured electrode provides an encouraging alternative for integration of high-performance micro-supercapacitors onto silicon chips, components in which per-area performance is critical.

Macroporous gold electrodes (*i.e.* with pore diameters greater than 50 nm) were prepared by electrodeposition onto evaporated gold thin films in the presence of hydrogen tetrachloroaurate ( $\text{HAuCl}_4 \cdot 4\text{H}_2\text{O}$ ) acidic solution. At a significant overpotential, vigorous hydrogen bubbling occurs on the surface, disturbing the diffusion layer and the localized current density. This affects the growth morphology and acts as a dynamic template. Scanning electron microscopy (SEM) images, **Figure 1a**, shows the representative results for porous gold deposits consisting of a honeycomb network with interconnected and cross-linked pores. The diameter of the largest pores varies between 20 to 40  $\mu\text{m}$  and pore size increases from the bottom to the top of the substrate. The internal wall structure of these larger pores is composed of multi-branched dendrites and nodules, with pores as small as 50 nm. Additional details on the influence of the electrodeposition parameters (initiation and growth times) required to obtain the features outlined in Figure 1 may be found in the Supporting Information (Figures S1 and S2). Figure 1b displays the corresponding steady state cyclic voltammograms (CV) obtained for gold substrate (1  $\text{cm}^2$  geometrical surface) before (black curve) and after electrodepositing the porous gold structure (orange curve). Both CVs exhibit the typical gold electrochemical response in sulphuric acid solution, with a double layer (from -0.2 to 0.5 V *vs.* SCE) and a gold oxide formation/reduction (from 0.6 to 1.6 V *vs.* SCE) potential regions. The gold oxide formation only occurs above 1.0 V *vs.* SCE, suggesting this layer has the electrochemical stability required for the subsequent  $\text{RuO}_2$  deposition and will provide good mechanical stability at long cycles. In the cathodic sweep, the magnitude of the Au oxide reduction peak, and thus the associated charge, centered at 0.8 V *vs.* SCE, is significantly higher for the porous Au electrode (92 mC) than the gold thin film (0.55 mC). An electrochemical active surface area (EASA) was determined based on the coulombic charge involved in such reduction process,<sup>[28]</sup> with reproducible values of 1.5  $\text{cm}^2$  and 230  $\text{cm}^2$  for the bare gold and the porous gold deposits, respectively.

Next, electrodeposition of the pseudo-capacitive hydrous ruthenium oxide  $\text{RuO}_2 \cdot x\text{H}_2\text{O}$  (Figure S3, Supplementary Information) onto the porous gold electrode was carried out from an aqueous ruthenium chloride  $\text{RuCl}_3 \cdot x\text{H}_2\text{O}$  solution by cyclic voltammetry.<sup>[29,30]</sup> From the SEM images (**Figure 2a** and Figure S4 in Supplementary Information), we note that the pseudo-capacitive hydrated  $\text{RuO}_2 \cdot x\text{H}_2\text{O}$  particles have been electrodeposited all along the nodule morphology of the porous layer, on the entire thickness from the bottom to the top of the substrate. As the gold surface is fully covered by  $\text{RuO}_2 \cdot x\text{H}_2\text{O}$ , the surface pore density is smaller and only the open porosity is observed. We then evaluated the electrochemical performances of the electrode made from porous gold current collector covered with  $\text{RuO}_2 \cdot x\text{H}_2\text{O}$  particles by using cyclic voltammograms (Figure 2b). In sulphuric acid, the CV of the porous Au/  $\text{RuO}_2 \cdot x\text{H}_2\text{O}$  electrode indicates a roughly rectangular shape, as expected for the electrochemical signature of pseudo-capacitive amorphous  $\text{RuO}_2 \cdot x\text{H}_2\text{O}$ , with excellent reversibility. The two quasi-symmetric peaks around 0.4 V vs. SCE originate from progressive change to the oxidation state of ruthenium, and the electrode exhibits an extremely high capacitance of 3,250 mF cm<sup>-2</sup> when cycled at 0.1 mV s<sup>-1</sup>. This represents a rather impressive value delivered by a micro-supercapacitor electrode, as displayed in the-state-of-the-art (see Table S1 in Supplementary Information). This extraordinary capacitance is reflected by a bit lower scan rate ability of the electrode compared with conventional supercapacitors.<sup>[31]</sup> To complete the study, the accessibility of charges has been investigated by calculating the voltammetric charge ( $q^*$ ) as a function of the sweep rates ( $\nu$ ), as described by Trasatti,<sup>[32,33]</sup> to identify the outer charge,  $q_{outer}$ , related to the more accessible active sites. The value of  $q_{outer}$  is obtained from the extrapolation of  $q^*$  to  $\nu = \infty$  (Figure 2c), whereas the total charge is estimated from the extrapolation of  $q^*$  to  $\nu = 0$  (Figure 2d). From these extrapolations, we obtained a  $q_{outer}$  value of 2.64 C cm<sup>-2</sup> (3.10 F cm<sup>-2</sup>) for a total charge of 2.95 C cm<sup>-2</sup> (3.47 F cm<sup>-2</sup>). Therefore,  $q_{outer}$  represents 90 % of the total charge, *i.e.* most of the full storable charge is rapidly accessible, fulfilling a substantial requirement for a

supercapacitor. The gravimetric capacitance of the  $\text{RuO}_2 \cdot x\text{H}_2\text{O}$  deposited onto the porous current collector is estimated to be very close to the theoretic value for hydrous Ru oxide.<sup>[34]</sup> The use of a 3D current collector improves the utilization efficiency of the ruthenium oxide and provides short transport/diffusion path lengths for protons and electrons. The equivalent series resistance (ESR) is also very low ( $1.83 \Omega \text{ cm}^2$ ) with a quasi-negligible high frequency semi-circle, as shown in the Nyquist plot (Figure S5, Supplementary Information). In the low-frequency region, a sharp increase of the imaginary portion of the impedance is observed with a nearly-vertical straight line, as is expected for capacitive behaviour with no leakage current.

To assess the performance of this electrode material in a device, we created an all-solid-state micro-supercapacitor in a stack configuration integrated on a silicon wafer, using a poly (vinyl alcohol)-based electrolyte doped with silicotungstic acid (SiWa). A remarkable cell capacitance of  $1,220 \text{ mF cm}^{-2}$  is determined from galvanostatic charge/discharge experiments (**Figure 3a**) with a very low IR-drop voltage ( $38 \text{ mV}$  at  $1.5 \text{ mA cm}^{-2}$ ). The delivered specific energy density estimated from this plot achieves a value of  $0.126 \text{ mWh cm}^{-2}$  ( $7.9 \text{ mWh cm}^{-3}$ ), and the maximum power density of  $7.9 \text{ mW cm}^{-2}$  ( $493.8 \text{ mW cm}^{-3}$ ). These results exceed the best devices in terms of specific power with rather impressive specific energy per surface area (see Table S1 in Supplementary Information). The significant capacitance retention, about 95 % after 2,000 cycles (Figure 3b), indicates the good cycle life stability for the device. This electrochemical stability hints that the morphology of the porous  $\text{Au/RuO}_2 \cdot x\text{H}_2\text{O}$  electrode is maintained during repetitive charge/discharge cycling. The structural characteristics of the porous current collectors, synthesized using the hydrogen bubble dynamic template route, provide a mechanical and conductive framework to obtain a durable three-dimensional  $\text{RuO}_2 \cdot x\text{H}_2\text{O}$ . The micro-supercapacitor also exhibits very low self-discharge, with less than  $0.01 \text{ V/hour}$  lost after charging (Figure 3c). The performances of the solid-state leakage-free micro-supercapacitor are finally demonstrated in a Ragone plot in comparison with commercial and state-of-the-art

micro-batteries as reported in the literature (Figure 3d).<sup>[35]</sup> This porous Au/RuO<sub>2</sub>.xH<sub>2</sub>O device is positioned remarkably well in terms of power density and lifetime compared to other devices, while its energy density is in the upper range of state-of-the-art micro-batteries and in the lower range of commercial Li-thin film batteries. In conclusion, with a cost of active material estimated to be less than 10 cents per mm<sup>2</sup>, this type of electrode material design is very promising for the integration of micro-supercapacitors in wearable electronic devices and self-powered microsystems, in which the key consideration is to minimize footprint occupancy while maximizing the energy. Further improvements in the micro-fabrication (with current collectors patterned in interdigital configurations) and electrodeposition process of the porous gold (like AuCu thin films dealloying) should also easily result in micro-devices with even higher areal energy.

## **Experimental Section**

*Electrode and Device Fabrication:* A Ti(100 nm)/Au(400 nm) thin film was deposited by evaporation on an oxidized silicon substrate and electrochemically pre-treated by cycling the potential at a scan rate of 100 mV s<sup>-1</sup> between -0.3 and 1.7 V vs. SCE in 1 M H<sub>2</sub>SO<sub>4</sub> until a stable voltammogram was obtained. Electrodeposition of the porous gold was then carried out, from an aqueous solution of 2 mM HAuCl<sub>4</sub>.4H<sub>2</sub>O in 2 M H<sub>2</sub>SO<sub>4</sub>, by applying a potential of -1.5 V vs. SCE for 3 minutes of initiation time, followed by 1 minute at open circuit and 40 minutes of deposition time. Electrodeposition of hydrous ruthenium oxide onto the porous Au was obtained by cycling the electrode between -0.3 and +0.9 V vs. SCE at 50 mV s<sup>-1</sup> and 50°C for 300 cycles in a stirring solution containing 5 mM RuCl<sub>3</sub>.xH<sub>2</sub>O in 10<sup>-1</sup> M KCl/10<sup>-2</sup> M HCl, adjusted to pH = 2.5 with a 2 M KOH aqueous solution. The electrode was then annealed at 150 °C for one hour. Next, the electrodes were used to design a solid-state device in a stacked configuration, separated by a membrane of cellulose nitrate impregnated with electrolyte. The solid polymer electrolyte was prepared by mixing a poly (vinyl alcohol)

(PVA,  $M_w = 31\,000\text{--}50\,000$ , 87-89% hydrolyzed) solution with phosphoric acid ( $\text{H}_3\text{PO}_4$ ) and SiWa ( $\text{H}_4\text{SiW}_{12}\text{O}_{40}$ ) in a composition of 1.7 wt% PVA, 1.9 wt%  $\text{H}_3\text{PO}_4$ , 14.4 wt% SiWa and 82 wt% de-ionized water.<sup>[36]</sup> The conductivity of the solid electrolyte was  $6.1\text{ mS cm}^{-1}$  after 24 h (22.2 °C - 32% RH).

*Characterizations:* The electrochemical characterizations were performed with a SP-240 BioLogic potentiostat. SEM images were obtained using a Hitachi S-4800 field emission electron microscope. The surface chemical composition of ruthenium oxide was estimated *via* X-ray Photoelectron Spectroscopy (XPS) using a Thermo Scientific spectrometer operating with a monochromatic Al  $K\alpha$  X-ray source (1486.6 eV).

## Acknowledgements

This work was partly supported by the French RENATECH network (D. Pech) and the Canada Research Chair program (D. Guay).

- [1] Z. L. Wang, *Adv. Mater.* **2012**, 24, 280.
- [2] J. G. Koomey, H. S. Matthews, E. Williams, *Annu. Rev. Environ. Resour.* **2013**, 38, 17.1.
- [3] X. Wang, X. Lu, B. Liu, D. Chen, Y. Tong, G. Shen, *Adv. Mater.* **2014**, 26, 4763.
- [4] M. Beidaghi, Y. Gogotsi, *Energy Environ. Sci.* **2014**, 7, 867.
- [5] J. J. Yoo, K. Balakrishnan, J. Huang, V. Meunier, B. G. Sumpter, A. Srivastava, M. Conway, A. L. Mohana Reddy, J. Yu, R. Vajtai, P. M. Ajayan, *Nano Lett.* **2011**, 11, 1423.
- [6] W. W. Liu, Y. Q. Feng, X. B. Yan, J. T. Chen, Q. J. Xue, *Adv. Funct. Mater.* **2013**, 23, 4111.
- [7] P. Huang, D. Pech, R. Lin, J. K. McDonough, M. Brunet, P. L. Taberna, Y. Gogotsi, P. Simon, *Electrochem. Commun.* **2013**, 36, 53.

- [8] P. Huang, M. Héon, D. Pech, M. Brunet, P. L. Taberna, Y. Gogotsi, S. Lofland, J. D. Hettinger, P. Simon, *J. Power Sources* **2013**, 225, 240.
- [9] T. M. Dinh, D. Pech, M. Brunet, A. Achour, *J. Phys.: Conf. Ser* **2013**, 476, 012106.
- [10] D. Pech, M. Brunet, P. L. Taberna, P. Simon, N. Fabre, F. Mesnilgrete, V. Conédéra, H. Durou, *J. Power Sources* **2010**, 195, 1266.
- [11] D. Pech, M. Brunet, H. Durou, P. Huang, V. Mochalin, Y. Gogotsi, P. L. Taberna, P. Simon, *Nature Nanotech.* **2010**, 5, 651.
- [12] Z. Peng, R. Ye, J. A. Mann, D. Zakhidov, Y. Li, P. R. Smalley, J. Lin, J. M. Tour, *ACS Nano* **2015**, 9, 5868.
- [13] T. Brousse, D. Bélanger, J. W. Long, *J. Electroche. Soc.* **2015**, 162, A5185.
- [14] W. Deng, X. Ji, Q. Chen, C. E. Banks, *RSC Adv.* **2011**, 1, 1171.
- [15] C. C. Liu, D. S. Tsai, S. Susanti, W. C. Yeh, Y. S. Huang, F. J. Liu, *Electrochim. Acta* **2010**, 55, 5768.
- [16] T. M. Dinh, K. Armstrong, D. Guay, D. Pech, *J. Mater. Chem. A* **2014**, 2, 7170.
- [17] S. Li, X. Wang, H. Xing, C. Shen, *J. Micromech. Microeng.* **2013**, 23, 114013.
- [18] B. L. Ellis, P. Knauth, T. Djenizian, *Adv. Mater.* **2014**, 26, 3368.
- [19] X. Lang, A. Hirata, T. Fujita, M. Chen, *Nature Nanotech.* **2011**, 6, 232.
- [20] J. Han, Y. C. Lin, L. Chen, Y. C. Tsai, Y. Ito, X. Guo, A. Hirata, T. Fujita, M. Esashi, M. Gessner, M. Chen, *Adv. Sci.* **2015**, 2, 1500067.
- [21] X. Wang, Y. Yin, X. Li, Z. You, *J. Power Sources* **2014**, 252, 64.
- [22] A. Ponrouch, S. Garbarino, D. Guay, *J. Power Source* **2013**, 221, 228.
- [23] W. Wang, S. Guo, I. Lee, K. Ahmed, J. Zhong, Z. Favors, F. Zaera, M. Ozkan, C. S. Ozkan, *Sci. Rep.* **2014**, 4, 4452.
- [24] T. M. Dinh, A. Achour, S. Vizireanu, G. Dinescu, L. Nistor, K. Armstrong, D. Guay, D. Pech, *Nano Energy* **2014**, 10, 288.

- [25] B. J. Plowman, A. P. O'Mullane, P. R. Selvakannan, S. K. Bhargava, *Chem. Commun.* **2010**, 46, 9182.
- [26] S. Cherevko, C. H. Chung, *Electrochem. Commun.* **2011**, 13, 16.
- [27] J. Liu, L. Cao, W. Huang, Z. Li, *ACS Appl. Mater. Inter.* **2011**, 3, 3552.
- [28] L. D. Burke, P. F. Nugent, *Gold Bull.* **1997**, 30, 43.
- [29] C. C. Hu, Y. H. Huang, *J. Electrochem. Soc.* **1999**, 146, 2465.
- [30] J. J. Jowa, H. J. Lee, H. R. Chena, M. S. Wu, T. Y. Wei, *Electrochim. Acta* **2007**, 52, 2625.
- [31] W. G. Pell, B. E. Conway, *J. Power Sources* **2001**, 96, 57.
- [32] S. Ardizzone, G. Fregorana, S. Trasatti, *Electrochim. Acta* **1990**, 35, 263.
- [33] J. Gaudet, A. Tavares, S. Trasatti, D. Guay, *Chem. Mater.* **2005**, 17, 1570.
- [34] C. C. Hu, W. C. Chen, K. H. Chang, *J. Electrochem. Soc.* **2004**, 151, A281.
- [35] J. H. Pikul, H. G. Zhang, J. Cho, P. V. Braun, W. P. King, *Nat. Commun.* **2013**, 4, 1732.
- [36] H. Gao, K. Lian, *J. Mater. Chem.* **2012**, 22, 21272.

**Figure 1.** Characterization of the porous gold current collector. a) SEM images at different magnifications of the porous gold showing different levels of pores. b) Cyclic voltammogram of the porous Au compared with a Au thin film, in de-aerated 0.5 M sulphuric acid. The electrochemically active surface area of the porous Au coating is 150 times larger than the Au thin film.

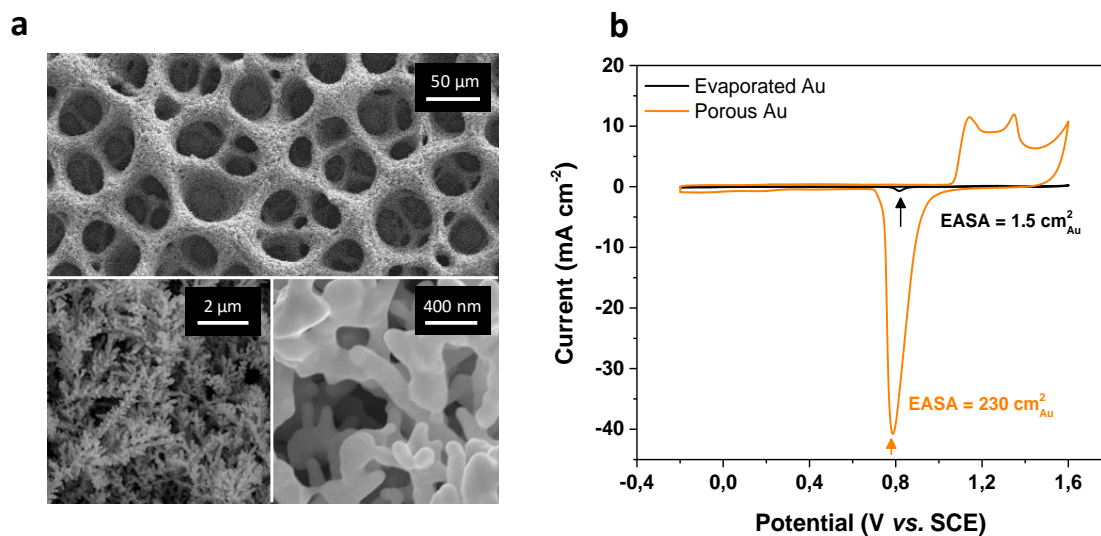


**Figure 2.** Characterization of the porous Au/RuO<sub>2</sub>.xH<sub>2</sub>O electrode. a) SEM images (top-view and cross-section) of the electrode obtained after 300 cycles of RuO<sub>2</sub> electrodeposition. b) Corresponding CV at 0.1 mV s<sup>-1</sup> in de-aerated 0.5 M sulphuric acid electrolyte. c) Determination of the outer capacitance ( $C_o$ ) of the electrode. d) Determination of the total capacitance ( $C_t$ ) of the electrode.

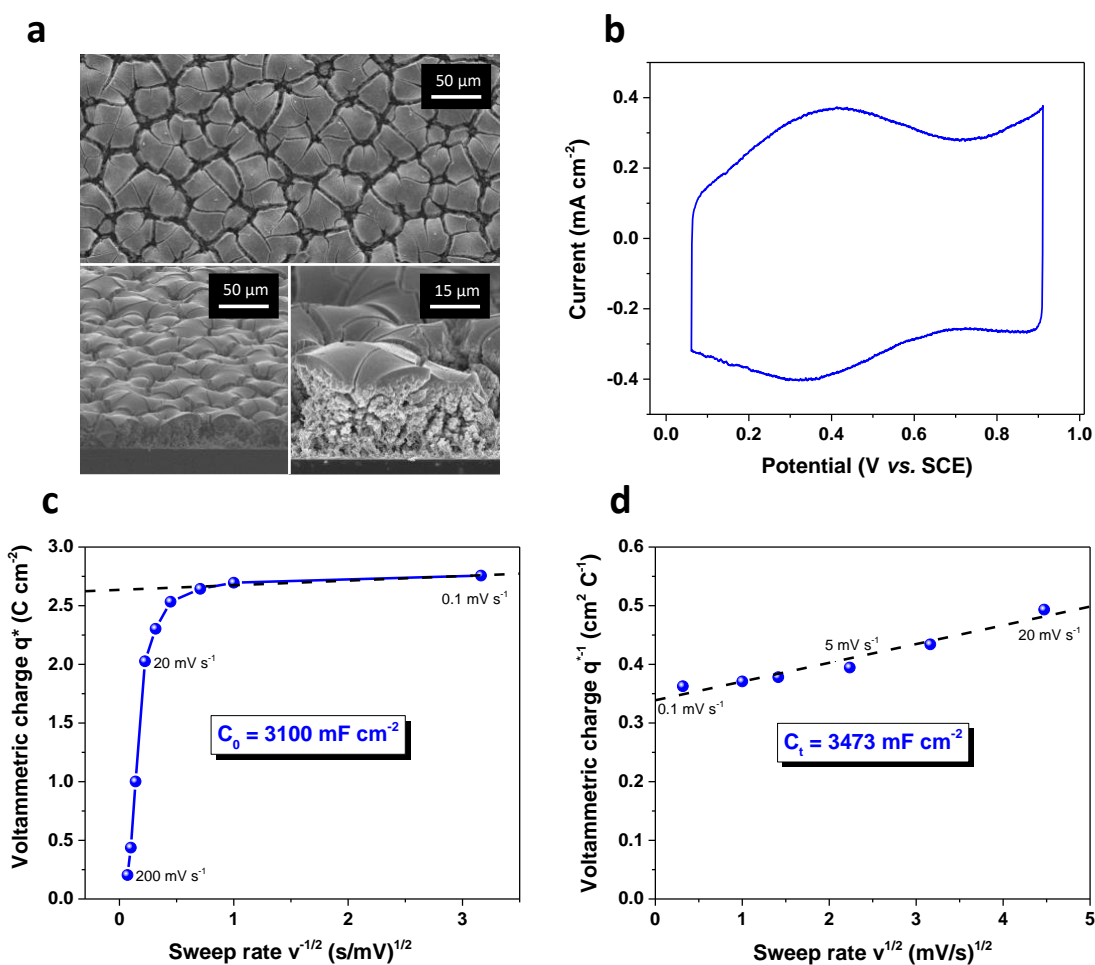


**Figure 3.** Characterization of the all-solid-state device. a) Galvanostatic charge/discharge curves at  $1.5 \text{ mA cm}^{-2}$ . b) Evolution of the relative capacitance vs. the number of charge/discharge curves cycles at  $1.5 \text{ mA cm}^{-2}$ . c) Measurement of the self-discharge rate. d) Ragone plot comparison of the specific energy and power per surface area of the porous Au/RuO<sub>2</sub>.xH<sub>2</sub>O-based micro-supercapacitor with state-of-the-art micro-batteries.

